Quasi-Free Electron States Responsible for Single-Molecule Conductance Enhancement in Stable Radical

Xingzhou Yang, Songjun Hou, Meiling Su, Qian Zhan, Hanjun Zhang, Sergio M. Quintero, Xiaodong Liu,* Junyang Liu, Wenjing Hong, Juan Casado, Qingqing Wu,* Colin J. Lambert,* and Yonghao Zheng*

AUTHOR INFORMATION

Xingzhou Yang - Department of Pharmacy, Sichuan Provincial People's Hospital, School of Optoelectronic Science and Engineering, University of Electronic Science and Technology of China, Chengdu 610072, People's Republic of China.

Songjun Hou - Department of Physics, Lancaster University, Lancaster LA1 4YB, UK.

Meiling Su - State Key Laboratory of Physical Chemistry of Solid Surfaces, College of Chemistry and Chemical Engineering, Xia-men University, Xiamen 361005, People's Republic of China.

Qian Zhan - Department of Pharmacy, Sichuan Provincial People's Hospital, School of Optoelectronic Science and Engineering, University of Electronic Science and Technology of China, Chengdu 610072, People's Republic of China.

Hanjun Zhang- Department of Pharmacy, Sichuan Provincial People's Hospital, School of Optoelectronic Science and Engineering, University of Electronic Science and Technology of China, Chengdu 610072, People's Republic of China.

Sergio M. Quintero - Department of Physical Chemistry, University of Málaga, Andalucia-Tech Campus de Teatinos s/n, Málaga 29071, Spain.

Junyang Liu - State Key Laboratory of Physical Chemistry of Solid Surfaces, College of Chemistry and Chemical Engineering, Xia-men University, Xiamen 361005, People's Republic of China.

Wenjing Hong - State Key Laboratory of Physical Chemistry of Solid Surfaces, College of Chemistry and Chemical Engineering, Xia-men University, Xiamen 361005, People's Republic of China.

Juan Casado - Department of Physical Chemistry, University of Málaga, Andalucia-Tech Campus de Teatinos s/n, Málaga 29071, Spain.

Corresponding Author

Xiaodong Liu - Department of Pharmacy, Sichuan Provincial People's Hospital, School of Optoelectronic Science and Engineering, University of Electronic Science and Technology of China, Chengdu 610072, People's Republic of China; E-mail: xdliu@uestc.edu.cn

Qingqing Wu - Department of Physics, Lancaster University, Lancaster LA1 4YB, UK; E-mail: q.wu6@lancaster.ac.uk

Colin J. Lambert - Department of Physics, Lancaster University, Lancaster LA1 4YB, UK; E-mail: c.lambert@lancaster.ac.uk

Yonghao Zheng - Department of Pharmacy, Sichuan Provincial People's Hospital, School of Optoelectronic Science and Engineering, University of Electronic Science and Technology of China, Chengdu 610072, People's Republic of China; E-mail: zhengyonghao@uestc.edu.cn

ABSTRACT Stable organic radicals, which possess half-filled orbitals in the vicinity of Fermi energy, are promising candidates for electronic devices. In this paper, using a combination of scanning-tunneling-microscope-based break junction (STM-BJ) experiment and quantum transport theory, stable fluorene-based radical is investigated. We demonstrate that the transport properties of a series of fluorene derivatives can be tuned by controlling the degree of localization of certain orbitals. More specifically, radical 36-FR has a delocalized half-filled orbital resulting in Breit-Wigner resonances, leads to an unprecedented conductance enhancement of two orders of magnitude larger than the neutral non-radical counterpart (36-FOH). In other words, conversion from a closed-shell fluorene derivative to the free radical in 36-FR opens an electron transport path which massively enhances the conductance. This new understanding of the role of radicals in single-molecule junctions, open up a novel design strategy for single-molecule-based spintronic devices.

TOC GRAPHICS

In single-molecule electronics research, all-organic conjugated radical species with unpaired electrons have attracted a lot of interest owing to their implications in the appearance of novel quantum phenomena, such as the reported molecules shown in Scheme 1. Van der Zant et al and Crivillers et al respectively found that the PTM radical (I) showed the Kondo effect[1] and long spin coherence times[2] in the single-molecule junction. Scheer and co-workers reported that the OPE radical exhibits magnetoresistive effects in a magnetic field, and its positive magnetoresistance is more than 1 order of magnitude larger than that of the non-radical state OPE[3]. In addition, organic radicals also have the potential to enhance electrical conductance[4-5]. Hong et al found that the conductance of PTZ-BT cation radical (II) is more than 200 times stronger than that of the non-radical neutral counterpart[5]. In a recent report, Vezzoli et al. demonstrated that the 6-oxoverdazyl derivatives (IV) retain their radical properties after the construction of single-molecule junctions, and the conductance of the 6-oxoverdazyl derivative increased by 1 order of magnitude compared to the non-radical precursor. Therefore, investigations of charge transport in single-molecule junctions are of great significance for future functional electronic devices, such as spintronic and recently for thermoelectric devices[6-15]. To date, extensive research efforts have been made to tune the properties of charge transport through single molecules by changing the molecular structure, environment and anchoring groups, introducing external stimuli, and using quantum interference (QI)[16-22].
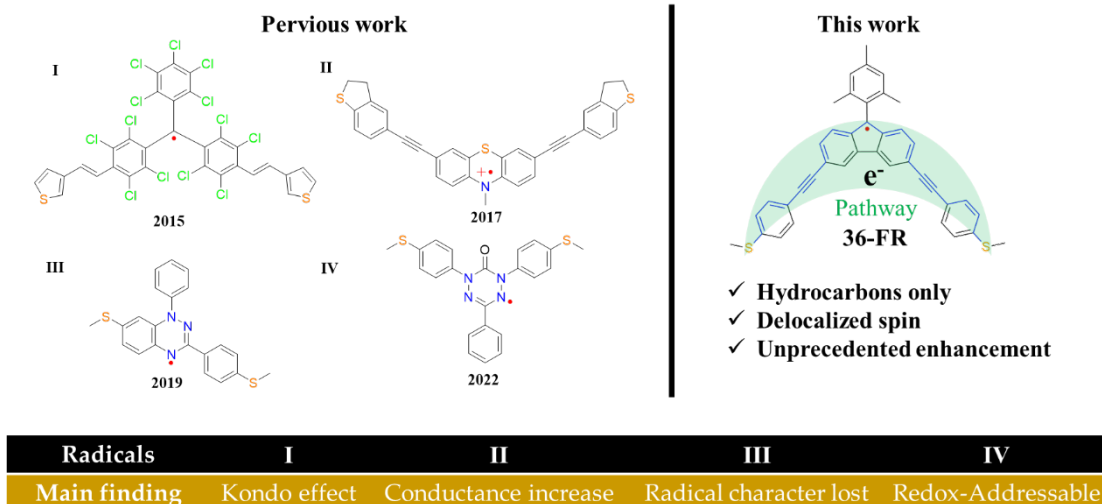
Scheme 1. A comparison between previous work and this work. (Left) Previous studies on stable radicals (I to IV) and their main founding. (Right) Molecule structure and properties of stable radical **36-FR** in this study.

Nevertheless, organic radicals are highly reactive due to the existence of unpaired electrons, and are usually very sensitive to external stimuli, such as moisture, oxygen, and heat[23-25]. Previous studies of charge transport in junctions containing a molecular radical were usually carried out under special conditions, such as high vacuum[3], and ultra-low temperature[1, 3]. In addition, in Venkataraman et al. study on Blatter radical (III), it was found that the radical character is also lost due to the charge transfer upon coupling of the molecule and the metal electrode in the solution-based single-molecule conductance measurements using scanning-tunnelling-microscope-based break junction (STM-BJ) method[26]. This indicates that the stability of radical states is endangered by the local environment around the molecule. To foresee the widespread use of radicals in various single-molecule electronic devices, the development of stable and persistent radicals at ambient conditions is mandatory[27]. Fluorene core gives a unique carbon only skeleton with multiple substituent sites, which provides a great opportunity to tune

the optical, electro- and spin- properties of the functional materials[15, 28-29]. Furthermore, fluorenyl-based neutral radicals show high stability under ambient conditions[30] owing to the rigid and planar, well conjugated and chemically robust aromatic ring structure of the closed-shell fluorene moiety, and are thus capable of promoting excellent charge transport features[31-32].

Herein, we design and synthesize closed-shell fluorene derivatives, **36-FO**, **36-FOH**, from which we further obtain their open-shell fluorenyl radical derivative **36-FR** (Scheme 2a). We measured the single-molecule conductance of all three compounds using the STM-BJ technique in 1,2,4-trichlorobenzene (TCB) solution at room temperature (Scheme 2b). Our experimental results show that the conductance varies from less than 10^{-7} G_0 in the non-radical molecule (**36-FOH**) up to $10^{-4.13}$ G_0 in the radical (**36-FR**). Density functional theory (DFT) and quantum transport calculations further illustrate that **36-FR** has a delocalized half-filled orbital resulting in Breit-Wigner resonances, which are responsible for the conductance difference between **36-FOH** (closed-shell) and **36-FR** radical (open-shell).
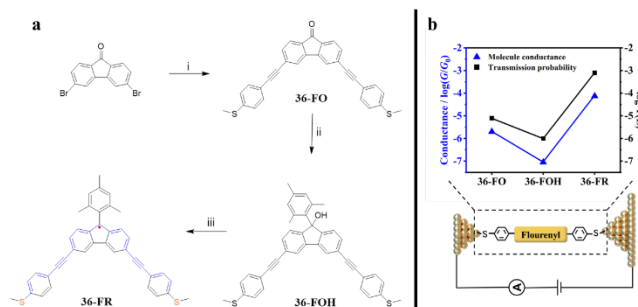
Scheme 2. (a) The synthetic routes of fluorene derivatives and radical. Reagents and conditions: (i) 1-ethynyl-4-methylsulfanylbenzene, Pd(PPh$_3$)$_4$, CuI, mixture of triethylamine (TEA) and N,N-Dimethylformamide (DMF), N$_2$ atmosphere, 90 ^{o}C; (ii) 2-mesitylmagnesium bromide (1 M solution in THF), dry THF, N$_2$ atmosphere, room temperature; (iii) anhydrous SnCl$_2$, trichloromethane, N$_2$ atmosphere, room temperature. (b) Schematic of STM-BJ setup and the

experimentally measured single-molecule conductance and the calculated transmission probability of fluorene derivatives.

Material synthesis and characterization. The synthetic route of the molecules studied is shown in scheme 2a. The detailed synthesis and characterization of the target molecules are described in Section S1 in Supporting Information. The target compounds can be obtained in good yields and were characterized by ^{1}H and ^{13}C nuclear magnetic resonance (NMR) (Figure S1 and Figure S3) and mass spectroscopy (Figure S2 and Figure S4).

Fourier transform infrared (FTIR) spectroscopy characterization showed the absorption peak of **36-FR** at 3506 cm^{-1} disappeared in comparison with **36-FOH**, indicating that there is no hydroxyl group at 9-position for **36-FR** sample, leads to high purity of radical (Figure 1a and Figure S7). Electron spin resonance (ESR) and UV-Vis-NIR absorption spectra were performed to confirm the generation of radicals in **36-FR** (Figures 1b and 1c and Figure S8). The ESR measurement was conducted in dry toluene at 295 K. For **36-FR,** an ESR signal with a *g* value of 2.004 can be clearly observed, which unambiguously verifies the existence of radicals in solution state (Figure 1b and Figure S9a). Furthermore, the UV-Vis absorption spectrum of **36-FR** showed a significant redshift compared to its precursors **36-FO** and **36-FOH**. In dichloromethane (DCM), the UV-visible absorption spectrum of **36-FO** and **36-FOH** are mainly concentrated in the near ultraviolet to 450 nm (Figure 1c and Figure S8). **36-FR** in DCM shows a strong absorption peak at 456 nm and a broad absorption band at 490-1000 nm (Figure 1c and Figure S9b), which are comparable to those observed in the previously reported fluorenyl radicals[30].

Furthermore, we examined the chemical stability of **36-FR** by monitoring the time evolution of its UV-Vis absorption spectra under ambient environments (Figure 1d and Figure S10). The 172

hours of monitoring showed that the absorption intensity steadily decreases with time. The absorption changes at 450 nm are fitted with exponential attenuation and the results show that the half-life of **36-FR** is approximately 335 hours (about 14 days), which suggests the excellent chemical stability of the **36-FR** radical.
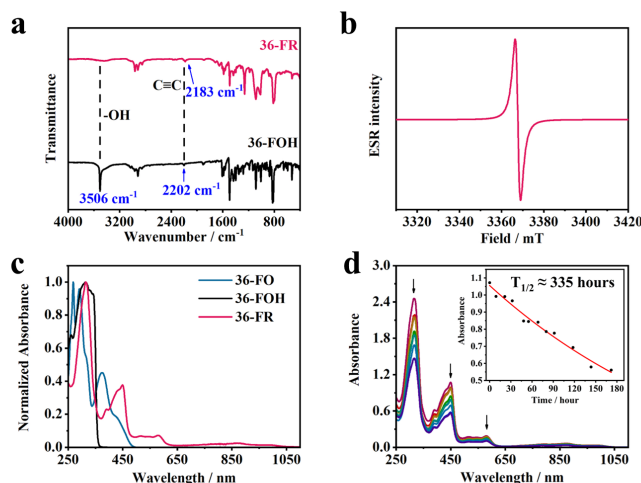

Figure 1. Material characterization. (a) FTIR transmission spectra of **36-FOH** (black) and **36-FR** (red). (b) ESR spectrum of **36-FR** in dry toluene. (c) Normalized absorption spectra of **36-FO, 36-FOH** and **36-FR** in DCM. (d) UV-Vis-NIR absorption spectra of **36-FR** (inset: exponential decay fitting of absorbance at 450 nm).

Single-molecule conductance measurements. The single-molecule conductance of the three compounds **36-FO**, **36-FOH** and **36-FR** in TCB solution were measured using the STM-BJ technique at room temperature in air, using a concentration of the target compound of 10^{-4} M and a bias voltage applied between the two electrodes of 0.1 V, as shown in scheme 2b. All results are obtained from more than 2000 individual traces, without any data selection (individual traces are shown in Figure S12).

Figure 2a, b shows the 2D conductance-displacement histograms of **36-FO** and **36-FR**, respectively, and Figure 2c presents the 1D conductance histograms of **36-FO** and **36-FR**.

The1D conductance histogram and 2D conductance-displacement histograms of **36-FO** are shown in Figure S14. From the 2D histograms, **36-FR** exhibits a distinct conductance step around 10^{-4} G_0, which shows a significant increase in conductance compared to **36-FO** and **36-FOH**. From the fitting results of the 1D histogram, **36-FR** discloses a clear peak at a conductance value of $10^{-4.17}$ G_0 (Figure 2b and Figure S13a), whereas **36-FO** has a small shoulder at *ca*. $10^{-5.54}$ G_0 (Figure 2a and Figure S13b). The 1D conductance histogram of **36-FOH** shows no obvious peaks (Figure S14a) suggesting an extremely low conductance value (we have tried to synthesis a shorter molecular length for higher conductance. However, with that particularly design, the target radical species was not formed.). On increasing the bias voltage to 0.5 V, the conductance signal of **36-FO** becomes more prominent with a Guassian-fitted histogram peak at $10^{-5.59}$ G_0 (Figure S15b). In contrast, **36-FOH** presents a low conductance shoulder at $10^{-7.05}$ G_0 (Figure S15c), which is in the limit of the instrument. Nonetheless, the conductance of **36-FO** is about 29 times higher than that of **36-FOH**; this is consistent with previous reports[33] which use either thiol and pyridyl as anchoring groups in *meta*-subsitituted fluorenes. In contrast, the conductance histogram of **36-FR** reveals a conductance value of $10^{-4.13}$ G_0 at 0.5 V bias (Figure S15a), which is around 800 times higher than that of **36-FOH**. Far surpasses the previous record of 200 times improvement set by the phenothiazine radical cation[5]. From the relative displacement distributions of **36-FO** and **36-FR** (insets of Figures 2c, d), the lengths of the molecular junctions are determined to be about 1.63 and 1.59 nm after adding the gold-gold snap-back distance of ~0.5 nm, in good agreement with the theoretically calculated molecular lengths of 1.73 nm and 1.77 nm. There is obvious change in relative displacement distribution for **36-FOH** (Figure S14b) compared with pure TCB, which indicates the successful formation of **36-FOH** molecular transport junction. Nevertheless, since the conductance signal of **36-FOH**

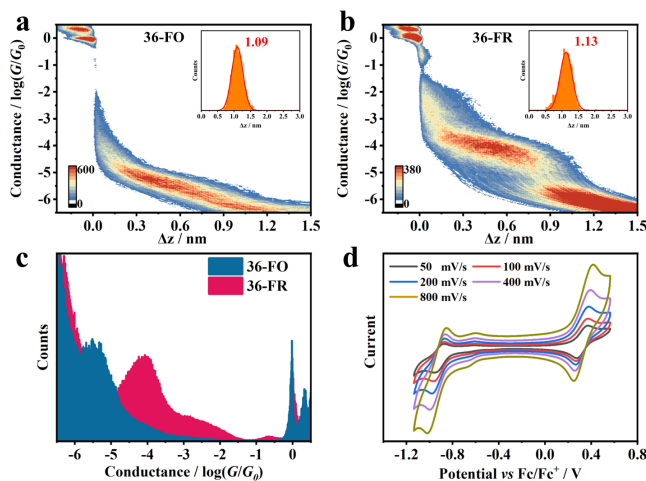is submerged by background noise, the lengths of the molecular junctions could not be resolved accurately.

Figure 2. Single-molecule conductance measurements and electrochemical measurements. 2D conductance-displacement histograms of (a) **36-FO** (N_{junc} = 2393) and (d) **36-FR** (N_{junc} = 3013). Insets show the corresponding relative displacement distribution histograms. (c) 1D conductance histograms of **36-FO** and **36-FR**. (d) Cyclic voltammograms of **36-FR** at different scan rates.

Previous work has shown that the Blatter radical with a low oxidation potential (about -0.29 V vs Fc/Fc⁺) easily loses its radical character in a single-molecule junction due to the facile charge transfer from the molecule to the gold electrode[26]. Therefore, high redox potentials of radicals are required for retaining its radical character when incorporated in a single-molecule junction. This is the case of reported by Naghibi *et al.* in which a 6-oxoverdazyl derivative can maintain its radical character in Au-molecule-Au junction owing to the high redox potential (+0.36 V vs Fc/Fc⁺ for oxidation potential and -1.03 V for reduction potential)[4]. Similarly, in the work of Frisenda *et al.*[1], it was also found that polychlorotriphenylmethyl (PTM) radical maintained a radical state due to its large redox potential. To ensure that **36-FR** still maintains its radical

character during the measurement of molecular junction conductance, we investigate the electrochemical properties of **36-FR** by cyclic voltammetry at different scan rates, as shown in Figure 2d (see Section S1 for more details). The cyclic voltammograms of **36-FR** exhibit similar shapes at various scan rates with a reversible one-electron oxidation wave and one-electron reduction wave at half-wave potentials of +0.32 V and -0.91 V vs Fc/Fc$^+$, respectively (Figure 2d), which suggests the excellent electrochemical stability of **36-FR**. The redox potentials of **36-FR** are close to those of 6-oxoverdazyl derivative reported in the literature[4], which indicates that **36-FR** can also maintain its radical state during the single-molecule junction measurement.
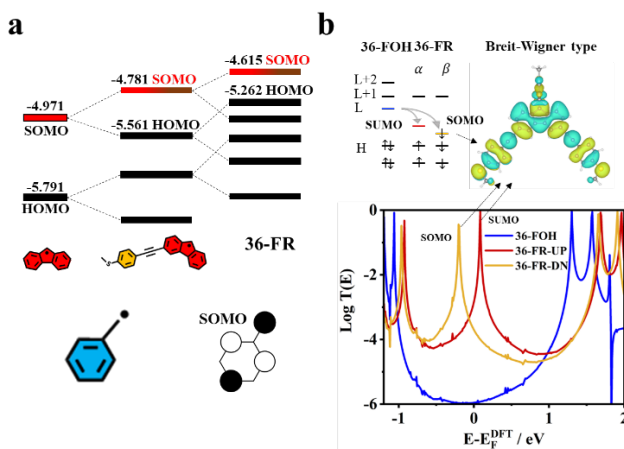

Figure 3. DFT calculation. (a) UDFT/B3LYP/6-311G(d) energy orbitals of **36-FR** showing the evolution from the starting fluorenyl radical. (b) Top: Energy diagram for **36-FOH** and **36-FR** (left panel) and SOMO and SUMO of **36-FR** (right panel). Bottom: Transmission spectra of **36-FOH** (blue curve) and **36-FR** (red for spin up and yellow for spin down). Energy levels HOMO-1, HOMO, LUMO, LUMO+1 and LUMO+2 are denoted as H-1, H, L, L+1 and L+2 for simplicity.

Transport Mechanisms and DFT calculations. To elucidate the observations in single-molecule conductance measurements, we carried out DFT calculations combined with quantum transport theory.

Electronic properties from calculations of the isolated molecule. Quantum chemical calculations at the UDFT/B3LYP/6-311G(d) level were carried out for the molecules as isolated entities in vacuum and the energies of their frontier molecular orbitals are shown in Figure 3a.

The orbital structure of **36-FR** is characterized by delocalized frontier orbitals involving the central fluorenyl encompassing the 9-p_z carbon orbital and the phenyl-acetylene arms. The only distinction is that the HOMO is a full delocalized orbital whereas the SOMO mostly spreads over the central part of the fluorene & phenyl-acetylene moieties, a common delocalization effect in the SOMO&HOMO that makes the former to appear in the middle HOMO-LUMO (lowest unoccupied molecular orbital) gap with a substantial SOMO-HOMO gap. The $sp^2 \rightarrow sp^3$ rehybridization of the 9-carbon atom in **36-FOH** affects all frontier molecular orbitals and alters the energies and topologies of all channels of electronic communication and transport.

These orbital features can be traced back to their molecular building blocks, as described in Figure 3a. The frontier orbitals of fluorenyl radical combine one-to-one upon perturbative bonding interaction with the branches, producing mixed fluorenyl/phenyl-acetylene molecular orbitals all with delocalized character.

Formally, abstraction of the hydroxyl radical of **36-FOH** creates a sp^2 hybridized carbon atom with a p_z orbital at the 9-carbon position that can be assimilated as a benzyl radical such as show in Figure 3a. The SOMO orbital of the benzyl radical at the Hückel level features a non-alternant, non-bonding character. The fluorenyl radical moiety can be considered as emerging from a benzyl fragment giving way to a similar SOMO orbital with important characteristics: **36-**

FR results from substitution in the *para*-positions relative to the 9-carbon radical, which now promotes strong electronic communication through the benzyl radical centre of the fluorene radical, a path that carries the main π-electron delocalization channel, thus leading to resonances of the Breit-Wigner type. In the same way, the inter-benzene 10,11 connection of **36-FR** is placed at *meta* position relative to the 3,6 connections and therefore is inactive as far electrical conductance is concerned. The existence of only one main π-path in **36-FR** means that this is fully blocked in **36-FOH,** which explains its null conductance in the STM-BJ experiment.

Quantum chemical calculations of transport properties. We find that the spin-degenerate LUMO of **36-FOH** is occupied by this excess electron, leading to a SOMO and a SUMO of **36-FR** (Figure 3b and Figure S17). In **36-FR**, two Breit-Wigner resonances emerge below and above the Fermi energy, which stem from the delocalized SOMO and SUMO (right panel of Figure 3b). Breit-Wigner formula provides simplest description of constructive quantum interference for an electron through a single molecular orbital[34]. As shown in Figure 3b, we see a significant increase due to the delocalized property of **36-FR** compared to **36-FOH**. It should be noted that DFT-predicted SOMO-SUMO gap depends on the exchange-correlation functionals adopted in the calculations. The gap is underestimated in the level of LDA functional which is utilized to calculate transmission function. Therefore, it can be expected that the trend of measured conductance among the different molecules at low bias is well predicted instead of the magnitudes.

We now examine the origin of the conductance discrepancy between **36-FO** and **36-FOH**. Figure S19 shows that in **36-FO**, the conductance enhancement is more pronounced compared to **36-FOH** which is ascribed to the smaller HOMO-LUMO gap induced by the downward (Figure S18) shifted LUMO of **36-FOH** (indicated by the black arrow in Figure S19) and the delocalized

LUMO (inset of Figure S19). Experimentally, the conductance of **36-FOH** is fully hidden in the background noise and a shoulder is observed for **36-FO** in the 1D conductance histogram shown in Figure 2c, demonstrating that the conductance of **36-FO** is higher than that of **36-OH**.

In this work, fluorene derivatives (**36-FO/FOH/FR**) are investigated by STM-BJ technique combined with quantum transport theory. The experimental results show that the single-molecule conductance of **36-FR** increases by about 800 times compared to that of **36-FOH** due to the delocalized frontier orbitals in **36-FR**, which is unprecedented in the field of single-molecule electronics. Through DFT calculations, we found that in comparison with non-radical molecules, the conductance enhancement of their radical counterparts is controlled by the degree of localization of the half-filled molecular orbital. More specifically, the delocalized half-filled orbital of **36-FR** leads to Breit-Wigner resonances close to Fermi energy, which gives rise to a much stronger conductance enhancement. This result suggests that the charge transport properties of radical molecular junctions can be tuned by intentionally controlling the degree of localization of their frontier orbitals, leading to a novel strategy for tuning their electrical conductance.

ASSOCIATED CONTENT

Supporting Information

The Supporting Information is available free of charge at

(I) Synthesis and characterization of fluorene derivatives and corresponding radicals. (II) STM-BJ Measurement. (III) Theoretical calculations. (IV) Coordinates for calculated geometries.

AUTHOR INFORMATION

Xingzhou Yang - School of Optoelectronic Science and Engineering, University of Electronic Science and Technology of China (UESTC), Chengdu 610054, People's Republic of China.

Songjun Hou - Department of Physics, Lancaster University, Lancaster LA1 4YB, UK.

Meiling Su - State Key Laboratory of Physical Chemistry of Solid Surfaces, College of Chemistry and Chemical Engineering, Xia-men University, Xiamen 361005, People's Republic of China.

Qian Zhan - School of Optoelectronic Science and Engineering, University of Electronic Science and Technology of China (UESTC), Chengdu 610054, People's Republic of China.

Hanjun Zhang- School of Optoelectronic Science and Engineering, University of Electronic Science and Technology of China (UESTC), Chengdu 610054, People's Republic of China.

Sergio M. Quintero - Department of Physical Chemistry, University of Málaga, Andalucia-Tech Campus de Teatinos s/n, Málaga 29071, Spain.

Junyang Liu - State Key Laboratory of Physical Chemistry of Solid Surfaces, College of Chemistry and Chemical Engineering, Xia-men University, Xiamen 361005, People's Republic of China.

Wenjing Hong - State Key Laboratory of Physical Chemistry of Solid Surfaces, College of Chemistry and Chemical Engineering, Xia-men University, Xiamen 361005, People's Republic of China.

Juan Casado - Department of Physical Chemistry, University of Málaga, Andalucia-Tech Campus de Teatinos s/n, Málaga 29071, Spain.

Corresponding Author

Xiaodong Liu - School of Optoelectronic Science and Engineering, University of Electronic Science and Technology of China (UESTC), Chengdu 610054, People's Republic of China; E-mail: xdliu@uestc.edu.cn

Qingqing Wu - Department of Physics, Lancaster University, Lancaster LA1 4YB, UK; E-mail: q.wu6@lancaster.ac.uk

Colin J. Lambert - Department of Physics, Lancaster University, Lancaster LA1 4YB, UK; E-mail: c.lambert@lancaster.ac.uk

Yonghao Zheng - School of Optoelectronic Science and Engineering, University of Electronic Science and Technology of China (UESTC), Chengdu 610054, People's Republic of China; E-mail: zhengyonghao@uestc.edu.cn

Notes

These authors contributed equally: X. Y., S. H. and M. S.

The authors declare no competing financial interests.

REFERENCES

(1) Frisenda, R.; Gaudenzi, R.; Franco, C.; Mas-Torrent, M.; Rovira, C.; Veciana, J.; Alcon, I.; Bromley, S. T.; Burzurí, E.; Van der Zant, H. S. J. Kondo effect in a neutral and stable all organic radical single molecule break junction. *Nano Lett*. **2015,** *15*, 3109-3114, DOI: 10.1021/acs.nanolett.5b00155.

(2) Bejarano, F.; Olavarria-Contreras, I. J.; Droghetti, A.; Rungger, I.; Rudnev, A.; Gutiérrez, D.; Mas-Torrent, M.; Veciana, J.; Van Der Zant, H. S. J.; Rovira, C.; Burzurı´, E.; Crivillers, N. Robust organic radical molecular junctions using acetylene terminated groups for C-Au bond formation. *J. Am. Chem. Soc*. **2018,** *140*, 1691-1696, DOI: 10.1021/jacs.7b10019.

(3) Hayakawa, R.; Karimi, M. A.; Wolf, J.; Huhn, T.; Zöllner, M. S.; Herrmann, C.; Scheer, E. Large magnetoresistance in single-radical molecular junctions. *Nano Lett*. **2016,** *16*, 4960-4967, DOI: 10.1021/acs.nanolett.6b01595.

(4) Naghibi, S.; Sangtarash, S.; Kumar, V. J.; Wu, J.-Z.; Judd, M. M.; Qiao, X.; Gorenskaia, E.; Higgins, S. J.; Cox, N.; Nichols, R. J.; Sadeghi, H.; Low, P. J.; Vezzoli, A. Redox-Addressable Single-Molecule Junctions Incorporating a Persistent Organic Radical. *Angew. Chem. Int. Ed*. **2022,** *61*, e202116985, DOI: 10.1002/anie.202116985.

(5) Liu, J.; Zhao, X.; Al‐Galiby, Q.; Huang, X.; Zheng, J.; Li, R.; Huang, C.; Yang, Y.; Shi, J.; Manrique, D. Z.; Lambert, C. J.; Bryce, M. R.; Hong, W. Radical-Enhanced Charge Transport in Single‐Molecule Phenothiazine Electrical Junctions. *Angew. Chem*. **2017,** *129*, 13241-13245, DOI: 10.1002/anie.201707710.

(6)   Xin, N.; Guan, J.; Zhou, C.; Chen, X.; Gu, C.; Li, Y.; Ratner, M. A.; Nitzan, A.; Stoddart, J. F.; Guo, X. Concepts in the design and engineering of single-molecule electronic devices. *Nat. Rev.* Phys. **2019,** *1*, 211-230, DOI: 10.1038/s42254-019-0022-x.

(7)   Zhen, S.; Mao, J.-C.; Chen, L.; Ding, S.; Luo, W.; Zhou, X.-S.; Qin, A.; Zhao, Z.; Tang, B. Z. Remarkable multichannel conductance of novel single-molecule wires built on through-space conjugated hexaphenylbenzene. *Nano Lett.* **2018,** *18*, 4200-4205, DOI: 10.1021/acs.nanolett.8b01082.

(8)   Hines, T.; Díez-Pérez, I.; Nakamura, H.; Shimazaki, T.; Asai, Y.; Tao, N. Controlling formation of single-molecule junctions by electrochemical reduction of diazonium terminal groups. *J. Am. Chem. Soc.* **2013,** *135*, 3319-3322, DOI: 10.1021/ja3106434.

(9)   Shen, P.; Huang, M.; Qian, J.; Li, J.; Ding, S.; Zhou, X. S.; Xu, B.; Zhao, Z.; Tang, B. Z. Achieving Efficient Multichannel Conductance in Through-Space Conjugated Single-Molecule Parallel Circuits. *Angew. Chem.* **2020,** *132*, 4611-4618, DOI: 10.1002/anie.202000061.

(10) Rocha, A. R.; García-suárez, V. M.; Bailey, S. W.; Lambert, C. J.; Ferrer, J.; Sanvito, S. Towards molecular spintronics. *Nat. Mater.* **2005,** *4*, 335-339, DOI: 10.1039/c8tc01399c.

(11) Gehring, P.; Sowa, J. K.; Hsu, C.; de Bruijckere, J.; van der Star, M.; Le Roy, J. J.; Bogani, L.; Gauger, E. M.; van der Zant, H. S. J. Complete mapping of the thermoelectric properties of a single molecule. *Nat. Nanotechnol.* **2021,** *16*, 426-430, DOI: 10.1038/s41565-021-00859-7.

(12) Shen, Y.; Xue, G.; Dai, Y.; Quintero, S. M.; Chen, H.; Wang, D.; Miao, F.; Negri, F.; Zheng, Y.; Casado, J. Normal & reversed spin mobility in a diradical by electron-vibration coupling. *Nat. Commun.* **2021,** *12*, 6262, DOI: 10.1038/s41467-021-26368-8.

(13) Wang, Y.; Tang, Z.; Chen, H.-Y.; Wang, W.; Tao, N.; Wang, H. Single-molecule calorimeter and free energy landscape. Proc. *Natl. Acad. Sci.* **2021,** *118*, e2104598118, DOI: 10.1073/pnas.2104598118.

(14) Hurtado-Gallego, J.; Sangtarash, S.; Davidson, R.; Rincón-García, L.; Daaoub, A.; Rubio-Bollinger, G.; Lambert, C. J.; Oganesyan, V. S.; Bryce, M. R.; Agraït, N.; Sadeghi, H. Thermoelectric Enhancement in Single Organic Radical Molecules. *Nano Lett*. **2022,** *22*, 948-953, DOI: 10.1021/acs.nanolett.1c03698.

(15) Yzambart, G.; Rincón-García, L.; Al-Jobory, A. A.; Ismael, A. K.; Rubio-Bollinger, G.; Lambert, C. J.; Agraït, N.; Bryce, M. R. Thermoelectric properties of 2, 7-dipyridylfluorene derivatives in single-molecule junctions. *J. Phys. Chem. C* **2018,** *122*, 27198-27204, DOI: 10.1021/acs.jpcc.8b08488.

(16) Baghernejad, M.; Van Dyck, C.; Bergfield, J.; Levine, D. R.; Gubicza, A.; Tovar, J. D.; Calame, M.; Broekmann, P.; Hong, W. Quantum Interference Enhanced Chemical Responsivity in Single-Molecule Dithienoborepin Junctions. *Chem. Eur. J.* **2019,** *25*, 15141-15146, DOI: 10.1002/chem.201903315.

(17) Jia, C.; Migliore, A.; Xin, N.; Huang, S.; Wang, J.; Yang, Q.; Wang, S.; Chen, H.; Wang, D.; Feng, B.; Liu, Z.; Zhang, G.; Qu, D.-h.; Tian, H.; Ratner, M. A.; Xu, H. Q.; Nitzan, A.; Guo, X. Covalently bonded single-molecule junctions with stable and reversible photoswitched conductivity. *Science* **2016,** *352*, 1443-1445, DOI: 10.1126/science.aaf6298.

(18) Guan, J.; Jia, C.; Li, Y.; Liu, Z.; Wang, J.; Yang, Z.; Gu, C.; Su, D.; Houk, K. N.; Zhang, D.; Guo, X. Direct single-molecule dynamic detection of chemical reactions. *Sci. Adv*. **2018,** *4*, eaar2177, DOI: 10.1126/sciadv.aar2177.

(19) Li, Z.; Smeu, M.; Ratner, M. A.; Borguet, E. Effect of anchoring groups on single molecule charge transport through porphyrins. *J. Phys. Chem. C* **2013,** *117*, 14890-14898, DOI: 10.1021/jp309871d.

(20) Yan, Z.; Li, X.; Li, Y.; Jia, C.; Xin, N.; Li, P.; Meng, L.; Zhang, M.; Chen, L.; Yang, J.; Wang, R.; Guo, X. Single-molecule field effect and conductance switching driven by electric field and proton transfer. *Sci. Adv*. **2022,** *8*, eabm3541, DOI: 10.1126/sciadv.abm3541.

(21) Zang, Y.; Fung, E.-D.; Fu, T.; Ray, S.; Garner, M. H.; Borges, A.; Steigerwald, M. L.; Patil, S.; Solomon, G.; Venkataraman, L. Voltage-induced single-molecule junction planarization. *Nano Lett*. **2020,** *21*, 673-679, DOI: 10.1021/acs.nanolett.0c04260.

(22) Yuan, L.; Jiang, L.; Nijhuis, C. A. The Drive Force of Electrical Breakdown of Large-Area Molecular Tunnel Junctions. *Adv. Funct. Mater*. **2018,** *28*, 1801710, DOI: 10.1002/adfm.201801710.

(23) Guo, Y.; Ding, S.; Zhang, N.; Xu, Z.; Wu, S.; Hu, J.; Xiang, Q.; Li, Z.-Y.; Chen, X.; Sato, S.; Wu, J.; Sun, Z. π-Extended Doublet Open-Shell Graphene Fragments Exhibiting One-Dimensional Chain Stacking. *J. Am. Chem. Soc*. **2022,** *144*, 2095-2100, DOI: 10.1021/jacs.1c12854.

(24) Ji, Y.; Long, L.; Zheng, Y. Recent advances of stable Blatter radicals: synthesis, properties and applications. *Mater. Chem. Front*. **2020,** *4*, 3433-3443, DOI: 10.1039/d0qm00122h.

(25) Hu, X.; Wang, W.; Wang, D.; Zheng, Y. The electronic applications of stable diradicaloids: present and future. *J. Mater. Chem. C* **2018,** *6*, 11232-11242, DOI: 10.1039/c8tc04484h.

(26) Low, J. Z.; Kladnik, G.; Patera, L. L.; Sokolov, S.; Lovat, G.; Kumarasamy, E.; Repp, J.; Campos, L. M.; Cvetko, D.; Morgante, A.; Venkataraman, L. The environment-dependent behavior of the blatter radical at the metal-molecule interface. *Nano Lett*. **2019,** *19*, 2543-2548, DOI: 10.1021/acs.nanolett.9b00275.

(27) Mas-Torrent, M.; Crivillers, N.; Rovira, C.; Veciana, J. Attaching persistent organic free radicals to surfaces: how and why. *Chem. Rev*. **2012,** *112*, 2506-2527, DOI: 10.1021/cr200233g.

(28) Guo, X.; Baumgarten, M.; Müllen, K. Designing π-conjugated polymers for organic electronics. Prog. *Polym. Sci*. **2013,** *38*, 1832-1908, DOI: 10.1016/j.progpolymsci.2013.09.005.

(29) Wong, W.-Y. Metallated molecular materials of fluorene derivatives and their analogues. *Coord. Chem. Rev*. 2005**,** *249*, 971-997, DOI: 10.1016/j.ccr.2004.10.007.

(30) Tian, Y.; Uchida, K.; Kurata, H.; Hirao, Y.; Nishiuchi, T.; Kubo, T. Design and synthesis of new stable fluorenyl-based radicals. *J. Am. Chem. Soc.* **2014,** *136*, 12784-12793, DOI: 10.1021/ja507005c.

(31) Lu, X.; Lee, S.; Kim, J. O.; Gopalakrishna, T. Y.; Phan, H.; Herng, T. S.; Lim, Z.; Zeng, Z.; Ding, J.; Kim, D.; Wu, J. Stable 3, 6-linked fluorenyl radical oligomers with intramolecular antiferromagnetic coupling and polyradical characters. *J. Am. Chem. Soc.* **2016,** *138*, 13048-13058.

(32) Zeng, Z.; Sung, Y. M.; Bao, N.; Tan, D.; Lee, R.; Zafra, J. L.; Lee, B. S.; Ishida, M.; Ding, J.; López Navarrete, J. T.; Zeng, W.; Kim, D.; Huang, K.-W.; Webster, R. D.; Casado, J.; Wu, J. Stable Tetrabenzo-Chichibabin's hydrocarbons: tunable ground state and unusual transition between their closed-shell and open-shell resonance forms. *J. Am. Chem. Soc.* **2012,** *134*, 14513-14525, DOI: 10.1021/ja3050579.

(33) Alanazy, A.; Leary, E.; Kobatake, T.; Sangtarash, S.; González, M. T.; Jiang, H.-W.; Bollinger, G. R.; Agräit, N.; Sadeghi, H.; Grace, I.; Higgins, S. J.; Anderson, H. L.; Nichols, R. J.; Lambert, C. J. Cross-conjugation increases the conductance of meta-connected fluorenones. *Nanoscale* **2019,** *11*, 13720-13724, DOI: 10.1039/c9nr01235d.

(34) Claughton, N.; Leadbeater, M.; Lambert, C. Theory of Andreev resonances in quantum dots. Journal *of Physics: Condensed Matter* **1995,** *7*, 8757, DOI: 10.1016/0039-6028(96)00408-6.